THE JOURNAL OF PHYSICAL CHEMISTRY C

Article

pubs.acs.org/JPCC

Origin of Enhancing the Photocatalytic Performance of TiO_2 for Artificial Photoreduction of CO_2 through a SiO_2 Coating Strategy

Lan Yuan,[†,‡] Chuang Han,[†,‡] Mario Pagliaro,[§] and Yi-Jun Xu*[,†,‡]

[†]State Key Laboratory of Photocatalysis on Energy and Environment, College of Chemistry, Fuzhou University, Fuzhou 350002, P. R. China

[‡]College of Chemistry, New Campus, Fuzhou University, Fuzhou 350108, P. R. China

[§]Istituto per lo Studio dei Materiali Nanostrutturati, CNR, via U. La Malfa 153, 90146 Palermo, Italy

Supporting Information

ABSTRACT: Artificial photosynthesis that mimics the natural photosynthetic protocol is now regarded as a promising candidate for chemical conversion of CO_2 to renewable solar fuels. In this work, core−shell structured TiO_2@SiO_2 composites have been synthesized via a simple sol−gel method under ambient temperature and pressure and applied to photocatalytic reduction of CO_2 with H_2O in the gas-phase under simulated solar light irradiation. The results show that compared with bare TiO_2, TiO_2@SiO_2 composites exhibit significantly enhanced adsorption capacity for CO_2 and facilitate photogenerated charge carrier separation and thereby enhanced photoactivity toward CO_2 reduction. Although the insulating nature of SiO_2 inhibits the charge injection from inner TiO_2 core through the silica layer to the outer surface, the separation efficiency of charge carriers within the inner pore structure of TiO_2@SiO_2 is facilitated due to the as-formed Ti−O−Si bonds. In particular, TiO_2@30%SiO_2, which balances the combined influence of CO_2 adsorption and charge carrier separation, acquires the best photoactivity and high selectivity for CO formation. This can be ascribed to the enriched density of adsorbed CO_2 and relatively lower electron density on the reactive sites of the samples. In addition, in contrast to bare TiO_2, the competitive process of H_2 formation is greatly inhibited over TiO_2@SiO_2 composites. It is hoped that our work could inspire ongoing interest in utilizing the SiO_2 coating method as well as other proper core−shell strategies to tune the activity and selectivity of semiconductor-based materials for artificial photoreduction of CO_2 to value-added solar fuels.

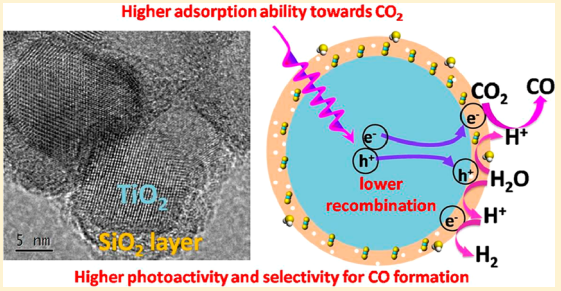

INTRODUCTION

Carbon dioxide (CO_2) in the atmosphere as a major greenhouse gas is causing mounting global environmental problems.[1−4] Intense research activities have been expended to develop technologies to facilitate the capture, sequester, and recycle of CO_2.[5−7] In particular, artificial photosynthesis that mimics the photosynthetic cycle of overall natural photosynthesis to convert CO_2 with H_2O into renewable hydrocarbon fuels by solar energy provides a sustainable way for carbon cycling, which is of great potential for solving both energy and environmental issues.[8−17] However, despite nearly 40 years' development, we are still very far from mimicking the complexity of natural photosynthetic centers for efficient photocatalytic reduction of CO_2.[2,5,13,18] The CO_2 conversion efficiency of artificial photosynthesis generally remains rather low, mainly because of the limited abilities of traditional semiconductors to activate thermodynamically stable CO_2 molecules.[19,20] Specifically, the initiation step of CO_2 activation, the first single-electron transfer from semiconductors to free CO_2, has a high electrochemical potential of −1.9 V vs NHE (normal hydrogen electrode) at pH = 7 and is the primary severe obstacle for the photoreduction of CO_2.[13,21,22]

To tackle this challenge, intense studies have been devoted to developing novel robust photocatalysts[23,24] or constructing strategies, such as band gap engineering, semiconductor combination, and cocatalyst loading to make the traditional photocatalysts powerful.[10,22,25,26] Recent researches have reported that enhancing adsorption of CO_2 on photocatalysts offers another way to activate the inert CO_2 molecule for further reduction.[21] The adsorbed CO_2 no longer has the linear symmetry of the free CO_2 molecule and its lowest unoccupied molecular orbital (LUMO) level decreases as the molecule bends, which is favorable for the electron transfer from excited photocatalysts to CO_2.[21,27,28] Therefore, strategies such as surface modification, nanostructuring, or dispersing the semiconductor to increase the surface area for CO_2 adsorption to enhance the activation of CO_2 are drawing increasing attention in recent years.[6,14,29−31]

The sol−gel silica coating strategy provides a green method to greatly increase the surface area of entrapped species to increase the adsorption capacity, with the advantages of being

Received: September 11, 2015
Revised: November 28, 2015
Published: December 1, 2015

DOI: 10.1021/acs.jpcc.5b08893
J. Phys. Chem. C 2016, 120, 265−273

one-step, having easy scale-up, being low cost, and being environmental friendly.[32,33] In particular, sol−gel silica is transparent to both visible and UV light irradiation and is known to be able to stabilize the entrapped species chemically and physically to tailor the properties and reactivity of the composites.[32−34] Specifically, it has been well investigated in the field of thermocatalysis that silica layers coated over catalytically active species could contribute to enhanced catalytic performance through stabilizing the catalyst nanoparticles, preventing their aggregation and providing large surface area to facilitate the mass transfer of the reactants.[35,36] However, reports concerning sol−gel entrapped semiconductors for enhanced photocatalysis remain relatively few. Only a limited number of studies in the field of photocatalytic dye degradation and organic synthesis have shown that the entrapment of semiconductor catalysts within sol−gel silica can contribute to enhanced photoactivity.[37−39] Yet, the research on sol−gel silica entrapped photocatalysts for gas-phase CO_2 photoreduction has not caused much concern.

Herein, we report the preparation of core−shell structured TiO_2@SiO_2 composites by coating SiO_2 over P25-TiO_2 via a simple sol−gel method under ambient temperature and pressure, investigation of its performance for photocatalytic CO_2 reduction with H_2O in gas-phase under simulated solar light irradiation, and the origin of enhanced photocatalytic performance through this simple coating strategy. The results show that the activity and selectivity for CO_2 photoreduction is able to be tuned by such a core−shell silica coating strategy. The TiO_2@SiO_2 composites exhibit higher photoactivity and selectivity for CO formation than bare TiO_2. Although the insulating nature of SiO_2 inhibits the charge injection from inner TiO_2 core through the silica layer to the outer surface, the separation efficiency of the charge carriers within the inner core−shell pore structure of TiO_2@$x$$SiO_2$ composites is facilitated due to the Ti−O−Si bonds formed in the core−shell TiO_2@$x$$SiO_2$ composites. Specifically, the highest activity is achieved over the TiO_2@30%SiO_2 sample, which can balance the integrative effect of the increased CO_2 adsorption ability and charge carrier separation. The higher selectivity for CO formation achieved over the TiO_2@SiO_2 composites can be ascribed to the enriched density of adsorbed CO_2 and relatively lower electron density on the reactive sites of the samples. In addition, the competitive process of H_2 formation from photocatalytic water splitting over TiO_2@SiO_2 is greatly inhibited. It is anticipated that our work could inspire ongoing interest in utilizing such a simple sol−gel silica coating strategy to tune the activity and selectivity of semiconductor-based materials for artificial photoreduction of CO_2 to valuable solar fuels.

EXPERIMENTAL SECTION

Catalyst Preparation. *Materials.* Degussa P25 (80% anatase titania and 20% rutile titania), tetraethylorthosilicate (TEOS, $Si(OC_2H_5)_4$, 99%), ethanol (EtOH), hydrochloric acid (HCl), and sodium hydroxide (NaOH) were used as received without further purification. Deionized (DI) water used in the synthesis process was obtained from local sources.

Synthesis. The core−shell structured TiO_2@$x$$SiO_2$ composites were prepared through the sol−gel method by entrapping certain amounts of TiO_2 within different weight ratio of silica matrices, which are obtained via the hydrolytic polycondensation of TEOS. Typically, (a) TEOS was hydrolyzed in the mixed solution of EtOH and HCl as the volume ratio of V(TEOS)/V(EtOH)/V(1 M HCl) = 1:2:1, stirring for 30 min; (b) 0.3 g of TiO_2 was ultrasonically treated in 1 mL of water for 30 min to obtain a well-dispersed TiO_2 suspension; (c) various amounts of TEOS solution obtained in step (a) were dropped into the TiO_2 suspension, stirring for another 30 min; (d) an aliquot of NaOH (1 M) aqueous solution was then added dropwise to the suspension to promote the condensation; (e) after feeding, the obtained suspension was aged in a closed vessel at room temperature for 24 h, and then dried at 60 °C for 3 days. The doped silica monolith thereby obtained was mildly powdered in a mortar and washed with distilled water several times until the ion concentration of the supernatant was <10 ppm. Ultimately, the precipitate was filtered and dried at 60 °C for further use, denoted as TiO_2@$x$$SiO_2$ (x = 5%, 10%, 30%, 50%). Blank SiO_2 was performed without the addition of P25 suspension, keeping other processes the same.

Catalyst Characterization. Transmission electron microscopy (TEM) images were obtained using a JEOL model JEM 2010 EX instrument at an accelerating voltage of 200 kV. X-ray photoelectron spectroscopy (XPS) measurements were performed on a Thermo Scientific ESCA Lab 250 spectrometer, which consists of monochromatic Al Kα as the X-ray source, a hemispherical analyzer, and a sample stage with multiaxial adjustability to obtain the surface composition of the samples. All of the binding energies were calibrated by the C 1s peak at 284.6 eV. The ^{29}Si NMR spectra were collected on a Bruker MSL 400 NMR spectrometer. The spinning rate was 4 kHz, and the number of scans was 512. Fourier transform infrared spectroscopy (FT-IR) was performed on a Nicolet Nexus 670 FT-IR spectrophotometer at a resolution of 4 cm^{-1}. The X-ray diffraction (XRD) patterns of the samples were collected on a Bruker D8 Advance X-ray diffractometer with Ni-filtered Cu Kα radiation at 40 kV and 40 mA in the 2θ range from 5° to 80° with a scan rate of 0.02° per second. The optical properties of the samples were analyzed by UV−vis diffuse reflectance spectroscopy (DRS) using a UV−vis spectrophotometer (Cary 500, Varian Co.), in which $BaSO_4$ was employed as the internal reflectance standard. Photoelectrochemical measurements were performed with a homemade three-electrode quartz cell with a PAR VMP3MultiPotentiostat apparatus. A Pt plate was used as the counter electrode, and a Ag/AgCl electrode was used as the reference electrode. The working electrode was prepared on fluoride tin oxide (FTO) conductor glass. Typically, the sample powder (5 mg) was ultrasonicated in 0.5 mL of DMF to disperse it evenly to obtain a slurry. The slurry was spread onto the FTO glass, whose side had been previously protected using Scotch tape. After air drying, the working electrode was further dried at 60 °C for 2 h to improve adhesion. A copper wire was connected to the side of the working electrode using conductive tape. Uncoated parts of the electrode were isolated with epoxy resin. Photocurrent measurements were taken on a BAS Epsilon workstation without bias, and the electrolyte was 0.2 M aqueous Na_2SO_4 solution (pH = 6.8) without additives. The electrochemical impedance spectroscopy (EIS) measurement was acquired via an EIS spectrometer (CHI-660D workstation, CH Instrument) in the three-electrode cell in the presence of 0.5 M KCl solution containing 5.0 mM $K_3[Fe(CN)_6]/K_4[Fe(CN)_6]$ by applying an AC voltage with 5 mV amplitude in a frequency range from 1 Hz to 100 kHz under open circuit potential conditions. The photoluminescence (PL) spectra for solid samples were investigated on an Edinburgh FL/FS920 spectrophotometer with an excitation wavelength of 380 nm. For PL decay measurements, the light-

DOI: 10.1021/acs.jpcc.5b08893
J. Phys. Chem. C 2016, 120, 265−273

emitting diode lamp was used to get the laser beam with excitation wavelengths of 340 nm. The 340 nm laser beam at an incident angle of ~45° relative to the normal direction was focused onto the samples at room temperature. Nitrogen adsorption−desorption isotherms and the Brunauer−Emmett−Teller (BET) surface areas were determined at 77 K using Micromeritics ASAP2010 equipment. The sample was degassed at 393 K for 5 h and then analyzed at 77 K. CO_2 adsorption isotherms were determined at 273 K using Micromeritics ASAP2010 equipment. The sample was degassed at 393 K for 5 h and then analyzed at 273 K.

Catalyst Activity. The photocatalytic reduction of CO_2 was performed in a gas−solid heterogeneous reaction mode in a quartz reactor (volume, ~25 mL; Figure S1). The loading mass of the photocatalyst sample was 20 mg. This system was evacuated by a mechanical pump and filled with pure CO_2 gas. The evacuation-filling operation was repeated three times. Evacuated liquid water (0.5 mL) was introduced finally with a syringe via the septum into the sample cell (5 mL) hanging in the quartz reactor, and the final pressure of CO_2 was kept as 8 kPa. A 300 W commercial Xe lamp (PLS-SXE 300, Beijing Perfectlight Co., Ltd.) was used as an irradiation resource of simulated solar light. The temperature of the reactor was kept at 298 K with an electronic fan. The photocatalytic reaction was typically performed for 8 h, and 0.3 mL of reactive gas was taken from the reactor with a syringe for analysis. The amounts of the products were analyzed by gas chromatography (GC 2014C) fitted with a high-sensitivity thermal conductivity detector (TCD) detector for quantifying the amounts of H_2 formed from H_2O photoreduction and a flame ionization detector (FID) detector for quantifying the amounts of CO and CH_4 formed from CO_2 photoreduction. After the effluents containing CO_2, H_2, CO and CH_4 were separated by a carbon molecular sieve (TDX-01) column, H_2 was analyzed by the TCD detector. CO was further converted to CH_4 by a methanation reactor and then analyzed by the FID detector. The amount of O_2 formed was quantified by Agilent 7890B equipped with 5A column and a TCD detector. The detection limits of our analytic method for CH_4 and CO were both 0.002 μmol. The detection limit for H_2 was 0.004 μmol. Argon was used as the carrier gas.

The products (O_2, H_2, CO, and CH_4) are measured directly by the evolved rate of the product within a certain time period under light irradiation by per gram of catalyst (eq A), provided that no other products are detected by the analysis of gas chromatography. The unit of R is μmol·$g_{catalyst}^{-1}$·h^{-1}. The conversion of CO_2 is calculated by the sum of the evolved rate of CO and CH_4 (eq B). The selectivity for CO is calculated using eq C.

$$R(O_2, H_2, CO, CH_4) = \frac{n(H_2, CO, CH_4)}{\text{time} \times m(\text{catalysts})} \quad \text{(A)}$$

$$\text{conversion of } CO_2 = R(CO) + R(CH_4) \quad \text{(B)}$$

$$\text{selectivity for CO} = \frac{2R(CO)}{2R(H_2) + 2R(CO) + 8R(CH_4)} \times 100\% \quad \text{(C)}$$

RESULTS AND DISCUSSION

The transmission electron microscopy (TEM) analysis of the samples has been carried out to get its microscopic structure information, as shown in Figure 1. It can be seen that most of the composite features the core−shell structure with the

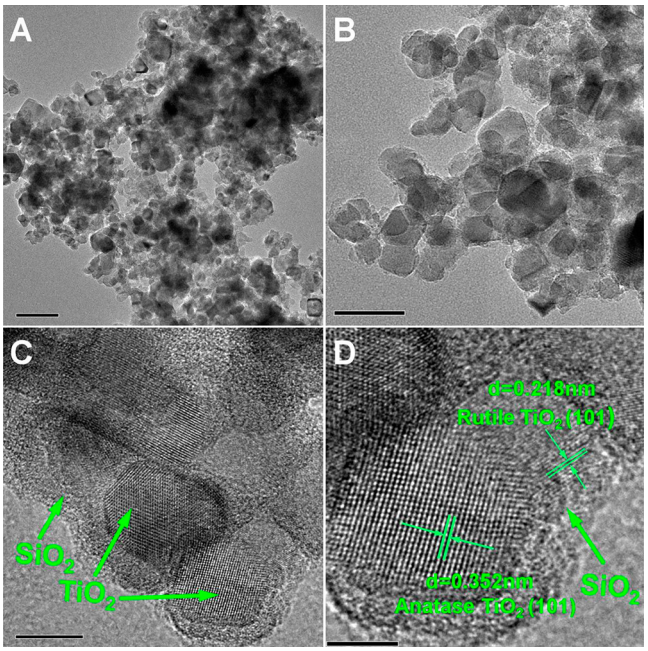

Figure 1. Typical transmission electron microscopy (TEM) images (A−C) and high resolution TEM (HRTEM) image (D) of TiO_2@30%SiO_2. Scale bar = 100, 50, 10, and 5 nm for A, B, C, and D, respectively).

amorphous SiO_2 shell coating the surface of TiO_2 (P25) nanoparticles. Since the surface of the P25-TiO_2 is hydrophilic and possesses a distribution of OH groups,[40] $Si(OH)_4$ molecules derived from the hydrolysis of TEOS could be easily adsorbed onto the surface layer of TiO_2 to form a shell.[33] Then, in the following processes of polycondensation, two or more molecules of $Si(OH)_4$ are condensed to form SiO_2, and the core−shell structured TiO_2@SiO_2 composite is formed.[32] The dimension distribution of the core and the shell for TiO_2@30%SiO_2 composites has been statistically estimated and presented in Figure S2, where the TiO_2 core displays the average diameter of ca. 20 nm, corresponding to the previously reported diameters of P25;[38] the thickness of the shell mainly ranges from 1.5 to 3.5 nm. The ordered crystal lattice fringes are shown in the HRTEM of Figure 1D, of which the spacing is measured to be equal to 0.352 and 0.218 nm, corresponding to the (101) crystal plane of anatase and rutile TiO_2, respectively.

The composition of SiO_2 shell and TiO_2 core in the TiO_2@SiO_2 composite can also be identified by X-ray photoelectron spectroscopy (XPS) measurements, an important method to investigate the chemical compositions and the existening forms of the elements in the samples.[41,42] The binding energies (BE) obtained in the XPS analysis have been calibrated for specimen charging by referencing C 1s to 284.6 eV (Figure 2A). In the region of Si 2p (Figure 2B), the BE of TiO_2@SiO_2 is equal to 103.4 eV, corresponding to the Si−O−Si bond,[39,43] while no such signal is detected in the BE of bare TiO_2, which suggests the formation of SiO_2 in TiO_2@SiO_2 composites.[44] In the region of O 1s (Figure 2C), the peaks appearing at 529.8, 531, and 531.8 eV are attributed to crystal lattice oxygen of TiO_2 (Ti−O), physically adsorbed oxygen, and hydroxyl group, respectively.[43,45,46] For TiO_2@SiO_2, another high peak located

DOI: 10.1021/acs.jpcc.5b08893
J. Phys. Chem. C 2016, 120, 265−273

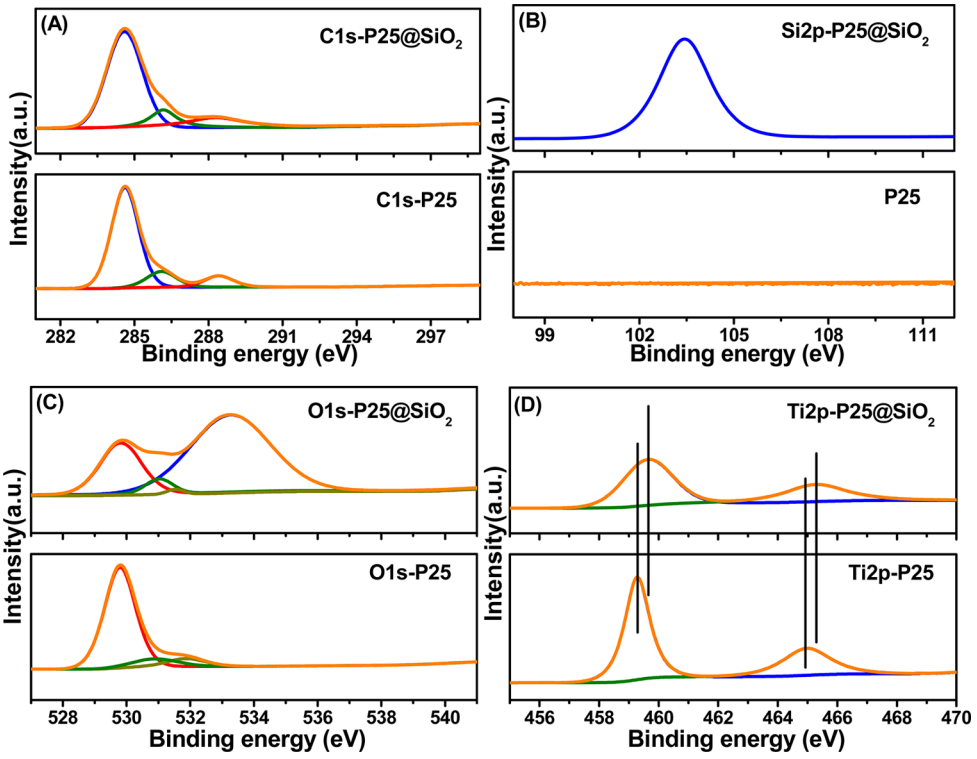

Figure 2. X-ray photoelectron spectroscopy (XPS) of TiO_2 and TiO_2@30%SiO_2 nanocomposites: C 1s as reference for calibration (A), Si 2p (B), O 1s (C), and Ti 2p (D).

at 533.3 eV is also ascribed to the Si−O−Si bond.[43,47] In the region of Ti 2p (Figure 2D), for bare TiO_2, two peaks located at 458.6 and 464.2 eV correspond to the BE of Ti $2p_{3/2}$ and Ti $2p_{1/2}$, respectively, indicating that the Ti element is present as the chemical state of Ti^{4+}.[43,48,49] As for TiO_2@SiO_2, the peak locations shift toward higher BE by 0.3 eV, manifesting that Ti−O−Si bond forms by the way of silicon substitution of titanium. The larger electronegativity of Si (1.8) than Ti (1.5) leads to the decrease of the electron density around Ti species and thus the effective positive charge on Ti increases, resulting in the increase of the BE of Ti 2p.[46,48] The combination of TEM and XPS results verifies that core−shell structured TiO_2@SiO_2 has been successfully fabricated by such a simple sol−gel approach.

Since the Si chemical shifts are sensitive to the second neighbor environment, ^{29}Si NMR has been employed to study the local structure between Si linkages in the TiO_2@SiO_2 composites.[50] It is known that SiO_2 exhibits signals corresponding to the resonance of Q^n (n = 0−4) species, which denotes a ^{29}Si nucleus with a $Si(SiO)_n(OX)_{4-n}$ local environment, where X represents H or Ti.[51] As for the ^{29}Si NMR spectrum of TiO_2@30%SiO_2 shown in Figure 3, three peaks at chemical shifts of −110.5, −101.1, and −91.8 ppm are mainly observed and assigned to Q^4, Q^3, and Q^2, respectively.[52] Q^4 sites are $[Si(SiO)_4]$ structural units for pure silica, indicating that the silica has a well-developed three-dimensional framework.[50] Q^3 sites can be attributed to contributions from both $Si(OSi)_3(OH)$ and $Si(OSi)_3(OTi)$, while Q^2 sites are from $Q^2[Si(SiO)_2(OH)_2]$ and $Q^2[Si(SiO)_2(OTi)_2]$, because OH and OTi groups have a similar influence on the central ^{29}Si nucleus.[52]

The chemical bonding between the TiO_2 core and SiO_2 shell of TiO_2@$xSiO_2$ composites is further investigated by the Fourier transform-infrared (FT-IR) spectra. As shown in Figure 4, the bands at 650, 1640, and 3480 cm^{-1} observed in all the samples correspond to Ti−O−Ti stretching vibration of

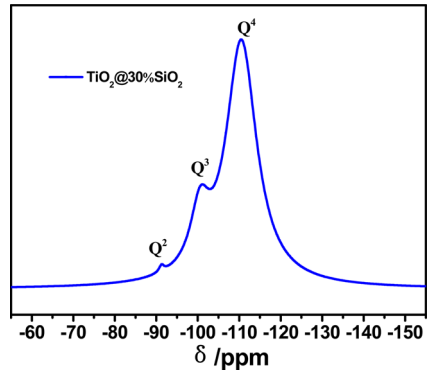

Figure 3. ^{29}Si NMR spectrum of TiO_2@30%SiO_2 composite.

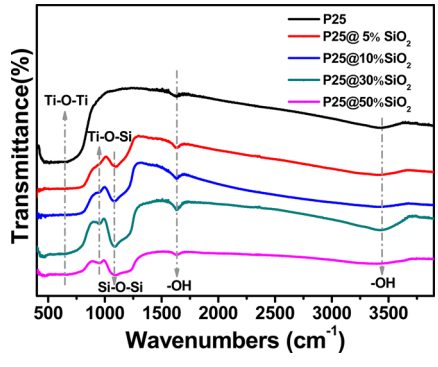

Figure 4. Fourier transform-infrared (FT-IR) spectra of TiO_2 and as-prepared TiO_2@$xSiO_2$ composites.

DOI: 10.1021/acs.jpcc.5b08893
J. Phys. Chem. C 2016, 120, 265−273

crystalline TiO_2 phase, the bending vibration of hydroxyl groups, and water, respectively.[53,54] Two other bands around 930 and 1080 cm^{-1} are shown in the spectra of all the TiO_2@$xSiO_2$ composites. The former is commonly accepted as the characteristic stretching vibration of Ti−O−Si bonds in Ti- and Si-containing catalysts, implying that the substitution of Si for Ti has occurred to form Ti−O−Si bonds in the composites,[54−57] which corresponds to the results of the XPS spectra. The latter corresponds to the asymmetric stretching vibration of Si−O−Si bonds in the SiO_2 shell.[53,54,57] The results further confirm the successful coverage of SiO_2 over the TiO_2 particles and verify the formation of Ti−O−Si bonds between SiO_2 and TiO_2 particles.

The X-ray diffraction (XRD) patterns have been obtained to study the crystal structures of the samples. As shown in Figure 5A, all the samples except bare SiO_2 are a mixture of anatase and rutile phases of TiO_2 particles, which agrees with the phase composition of Degussa P25 (approximately 80% anatase and 20% rutile).[58−60] And the good crystallinity of TiO_2 is well maintained during such a simple sol−gel preparation process at ambient conditions. One broad peak at ca. 23° can be observed for the TiO_2@$xSiO_2$ composites with high weight ratios of SiO_2 (30%, and 50%), which corresponds to the bare silica with amorphous structure.[61,62] This broad peak is quite weak and cannot be detected for TiO_2@$xSiO_2$ with low SiO_2 weight ratio, which could be due to its relatively weak diffraction intensity.[60] Diffuse reflection spectra (DRS) analyses have been implemented to explore the influence of the silica shell on the optical properties of the samples. As shown in Figure 5B, the absorption edges around 410 nm are observed for all the samples. Almost no obvious changes are observed in both UV and visible light region for the optical absorption of the TiO_2@$xSiO_2$ composites as compared with bare TiO_2. These suggest that the coating of SiO_2 layer over the TiO_2 surface does not result in significant loss of light absorption of TiO_2, which is because of the high optical transparency of SiO_2.

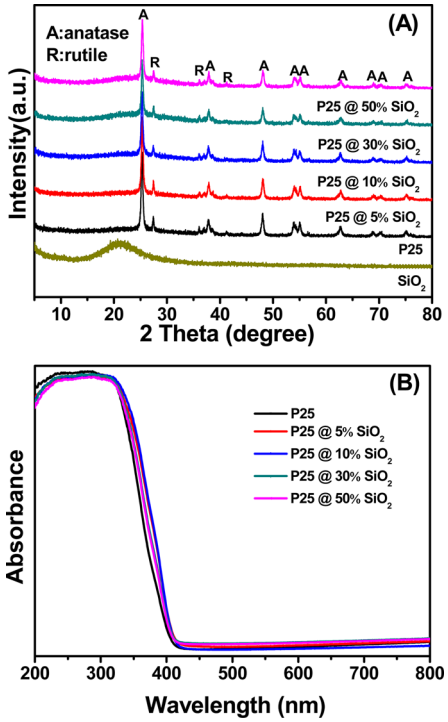

Figure 5. (A) X-ray diffraction (XRD) patterns and (B) UV−vis diffuse reflectance spectra (DRS) for TiO_2 and TiO_2@$xSiO_2$ composites.

After establishing successful coverage of SiO_2 layer over TiO_2, we have examined the photocatalytic performance of TiO_2 and TiO_2@$xSiO_2$ composites toward the photoreduction of CO_2 with H_2O under simulated solar light irradiation. Figure 6A shows the product distribution after 8 h light irradiation,

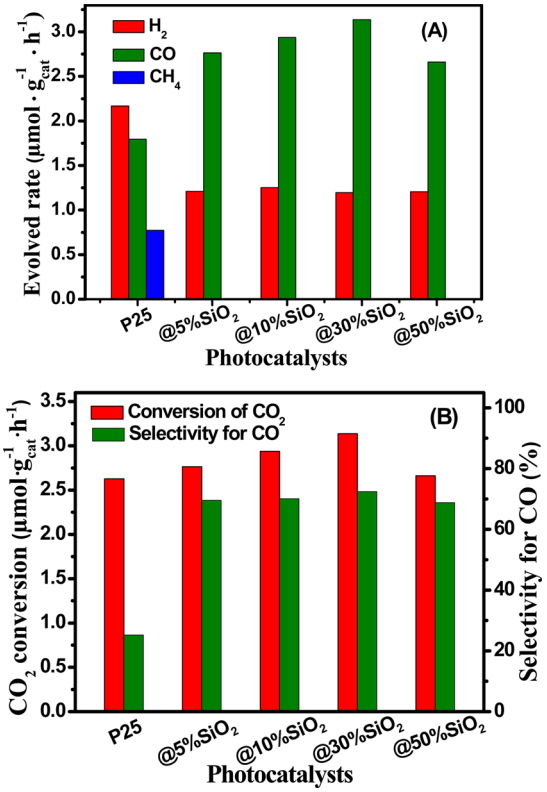

Figure 6. (A) The product distribution in the photocatalytic reduction of CO_2 with H_2O over TiO_2 and TiO_2@$xSiO_2$ composites. (B) The total conversion amount of CO_2 and the selectivity of CO versus H_2 and CH_4. Reaction conditions: 20 mg of catalysts, 0.5 mL of water, 8 kPa CO_2, 8 h of irradiation under simulated solar light.

and it is clear to see that in comparison with bare TiO_2, the photocatalytic reduction of CO_2 into CO is remarkably enhanced and the production of CH_4 is almost completely inhibited over TiO_2@$xSiO_2$ composites. In addition, the photoreduction of H_2O to H_2, the competitive reaction with the reduction of CO_2, has been efficiently inhibited over TiO_2@SiO_2 composites. Figure 6B clearly demonstrates that TiO_2@30%SiO_2 exhibits the highest conversion among all the samples. In particular, the selectivity of CO_2 photoreduction to CO is significantly improved, where TiO_2@30%SiO_2 attains the highest selectivity of 72.4%, which is nearly three times as that of bare TiO_2 (25.2%).

To understand how the SiO_2 layers influence the photocatalytic activity and selectivity toward reduction of CO_2, we have mainly investigated the structure−photocatalytic performance relationship in terms of joint analysis on surface area and the lifetime of photogenerated electron−hole pairs. The structure properties for the series of samples obtained from the N_2 adsorption−desorption and CO_2 adsorption experiments are summarized in Table S1, and it is clear to see that the BET surface areas for TiO_2@$xSiO_2$ composites are increased

DOI: 10.1021/acs.jpcc.5b08893
J. Phys. Chem. C 2016, 120, 265−273

with the content of SiO_2 increases, among which the average surface area of TiO_2@30%SiO_2 (92 m^2/g) and TiO_2@50%SiO_2 (95 m^2/g) nearly attain twice the values of bare TiO_2 (57 m^2/g). Figure S3 shows the representative N_2 adsorption−desorption isotherms of the samples, all of which exhibit characteristic features of type IV isotherms with a type H2 hysteresis loop, which is associated with a typical mesoporous structure.[63] Compared with bare TiO_2, the total pore volumes of TiO_2@$x$$SiO_2$ composites increase with the content of SiO_2 from 0.23 cm^3/g (TiO_2) to 0.51 cm^3/g (TiO_2@50%SiO_2), and the average pore size of the samples enlarges from 15 nm (TiO_2) to 27 nm (TiO_2@50%SiO_2). Additionally, Figure 7 displays the CO_2 adsorption isotherms of the TiO_2 and TiO_2@$x$$SiO_2$ samples, and it can be seen that the bare TiO_2 only exhibits CO_2 uptakes of 6.91 cm^3/g and the values keep increasing with the SiO_2 content, of which the maximum CO_2 uptake for TiO_2@50%SiO_2 reaches 16.89 cm^3/g, nearly three times as that of bare TiO_2 (Table S1). The results suggest that the coverage of SiO_2 over TiO_2 can significantly enhance the surface area and CO_2 adsorption ability of the photocatalysts, which is desirable to be able to facilitate the mass transfer process of CO_2 on the catalyst as well as the activation of CO_2, thus contributing to enhanced photocatalytic performance for CO_2 reduction.[64]

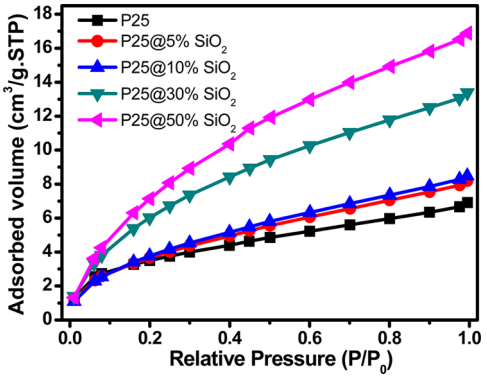

Figure 7. CO_2 adsorption isotherms (1 atm, 273 K) of TiO_2 and TiO_2@$x$$SiO_2$ composites.

The effect of electronic interaction between the SiO_2 coating layer and the TiO_2 core on photoelectrochemical properties of the samples has been investigated by electrochemical impedance spectroscopy (EIS) and transient photocurrent response analysis. As shown in Figure 8A, the Nyquist plots for bare TiO_2 and TiO_2@$x$$SiO_2$ electrodes all display semicycles at high frequencies and the diameter of the arc radius, which corresponds to the resistance of the electrodes, increases with the content of SiO_2. Figure 8B displays the transient photocurrent response of the TiO_2 and TiO_2@$x$$SiO_2$ electrodes over several on−off cycles of intermittent light irradiation. An obviously decreased transient photocurrent response of TiO_2@$x$$SiO_2$ can be observed compared with bare TiO_2, and the larger the coating amount of SiO_2, the weaker the photocurrent is. The photoelectrochemical results indicate that the coverage of SiO_2 layer over TiO_2 leads to an increase in the charge transfer resistance at the sample/electrolyte interface due to the insulating nature of SiO_2, which prohibits the charge injection from inner TiO_2 core through the silica layer to the outer surface.[48,65,66]

On the other hand, the photoluminescence (PL), a useful technique to investigate the charge transfer within a specific semiconductor photocatalyst,[37] is employed to elucidate the charge carrier recombination behavior within the TiO_2@$x$$SiO_2$ composites. It is well-known that following the electron−hole pair recombination after a photocatalyst is irradiated, photons are emitted, resulting in PL signal, the intensity of which provides a direct, qualitative measurement of the recombination rate of charge carriers. Lower peak intensities imply that a larger amount of photogenerated electrons are trapped and efficiently transferred, while high peak intensities indicate the occurrence of rapid charge recombination.[10,37,67,68] Figure 9 shows the PL

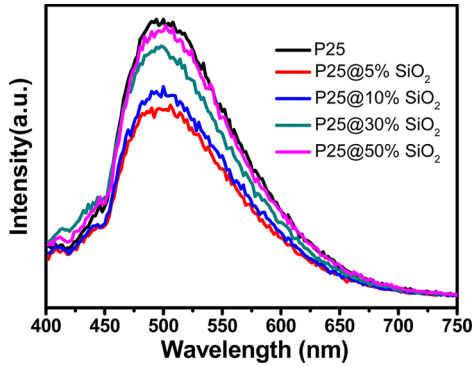

Figure 9. Photoluminescence emission spectra of TiO_2 and TiO_2@$x$$SiO_2$ composites.

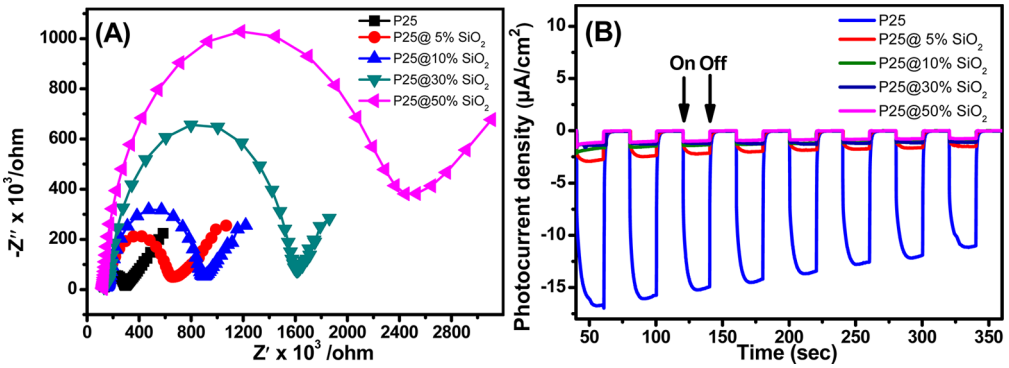

Figure 8. (A) Electrochemical impedance spectroscopy (EIS) Nyquist plots of TiO_2 and TiO_2@$x$$SiO_2$ electrodes in 0.5 M KCl solution containing 5.0 mM $K_3[Fe(CN)_6]/K_4[Fe(CN)]_6$. (B) Simulated solar light photocurrent−voltage curves of TiO_2 and TiO_2@$x$$SiO_2$ electrodes in 0.2 M Na_2SO_4 (pH = 6.8) aqueous solution versus Ag/AgCl electrode.

DOI: 10.1021/acs.jpcc.5b08893
J. Phys. Chem. C 2016, 120, 265−273

spectra of the samples, and it is clear to see that the PL intensity of all TiO_2@$xSiO_2$ composites is lower than that of non-entrapped TiO_2, among which TiO_2@5%SiO_2 exhibits the lowest PL intensity. The results suggest that compared with bare TiO_2, the recombination of charge carriers within the TiO_2@$xSiO_2$ composites is effectively inhibited. In order to figure out the lifetimes of the charge carriers within the photocatalysts, the photoluminescence decays of the samples are further measured. Table S2 displays the PL lifetimes of the samples, which are calculated through the exponential fit to the experimental data. It can be seen that all the TiO_2@$xSiO_2$ composites exhibit longer PL lifetimes than the bare TiO_2, among which TiO_2@5%SiO_2 presents the longest PL lifetime, while further increasing the coating amount of SiO_2 leads to decreased lifetimes. The order of the PL lifetimes of the series of TiO_2@$xSiO_2$ composites is TiO_2@5%SiO_2 > TiO_2@10%SiO_2 > TiO_2@30%SiO_2 > TiO_2@50%SiO_2 > P25, which is in accordance with the result of PL spectra. The above PL and PL lifetime results indicate that the charge carrier separation within the TiO_2@$xSiO_2$ composites is more efficient than that within bare TiO_2, which could be due to the formation of Ti−O−Si bridging bonds in the core−shell TiO_2@$xSiO_2$ composites. Such an effect has been observed over the non-core−shell composite photocatalyst consisting of ruthenium (Ru) doped anatase TiO_2 supported on silica, which are prepared by the solid-state dispersion method. Therein, it has been disclosed that the inhibition of the formation of the Ti−O−Si bonds by doping with Ru is detrimental to the charge carriers separation.[21,54] Specifically, TiO_2@5%SiO_2 composite with the smallest coating amount of SiO_2 is the optimal component construction for attaining the best charge carriers separation efficiency.

The combination of the photoelectrochemical properties and PL results indicate that although coating SiO_2 layer over TiO_2 is disadvantageous for the separation and transfer of photo-induced electron−hole pairs to the outer surface of the sample, the separation efficiency of the charge carriers within the inner pore structure of core−shell TiO_2@$xSiO_2$ composites is still facilitated due to the Ti−O−Si bonds formed in the as-prepared TiO_2@$xSiO_2$ composites.

Thus, the above results suggest that the CO_2 adsorption and charge carrier separation should have a synergistic effect on the performance of CO_2 photoreduction, which rationalizes the best photoactivity for CO_2 reduction achieved neither over TiO_2@50%SiO_2 with the highest CO_2 adsorption capacity nor TiO_2@5%SiO_2 with the most efficient charge carrier separation efficiency. It is the TiO_2@30%SiO_2, which could balance the combined influence of the CO_2 adsorption and charge carrier separation, that acquires the best photoactivity performance. Such a synergistic effect of increased CO_2 adsorption ability and lengthened lifetimes of the charge carriers over TiO_2@SiO_2 composites may also account for the selectivity tuning in the CO_2 photoreduction compared with that over bare TiO_2. As schematically shown in Figure 10, under simulated solar light irradiation, TiO_2 are photoexcited by the UV-part of the light to produce electrons (e^-) and holes (h^+) (eq 1). In the case of core−shell TiO_2@SiO_2, the electrons can diffuse to inner porosity of the silica cages where they can react with the adsorbed and incoming CO_2 molecules, and the facilitated separation of the charge carriers favors the proceeding of the photocatalytic redox reactions. The H_2O vapor, which acts as a sacrificial electron donor, undergoes oxidation to release O_2 (Table S3) and protons (H^+) (eq 2), with which CO_2 and the

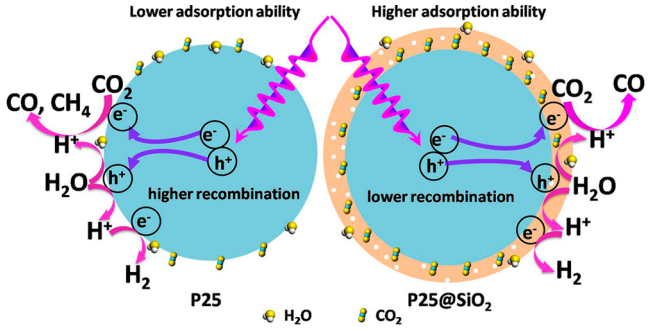

Figure 10. Illustration of the possible reaction mechanism for photocatalytic reduction of CO_2 with H_2O over TiO_2 and TiO_2@SiO_2 composite.

corresponding number of electrons interact and produce CH_4 (eq 3) or CO (eq 4). A competing reaction is that the H^+ can react with e^- to be reduced to H_2 (eq 5). Compared with bare TiO_2, TiO_2@SiO_2 can adsorb more CO_2, which has higher probability to be reduced, and thus efficiently suppresses the formation of H_2. In particular, it is well-known that the formations of CO and CH_4 require two and eight electrons, respectively. In the case of TiO_2@SiO_2, the enriched density of adsorbed CO_2 and the thus relatively lower electron density favor the formation of CO, leading to higher selectivity of photocatalytic reduction of CO_2 to CO. In brief, the synergistic interaction of TiO_2 with the SiO_2 layer plays a crucial role in affecting the activity and selectivity for the photoreduction of CO_2 over TiO_2@SiO_2 composites.

$$TiO_2 \rightarrow e^- + h^+ \quad (1)$$

$$H_2O + 2h^+ \rightarrow 1/2O_2 + 2H^+ \quad (2)$$

$$CO_2 + 8H^+ + 8e^- \rightarrow CH_4 + 2H_2O \quad (3)$$

$$CO_2 + 2H^+ + 2e^- \rightarrow CO + H_2O \quad (4)$$

$$2H^+ + 2e^- \rightarrow H_2 \quad (5)$$

CONCLUSIONS

Core−shell structured TiO_2@SiO_2 composites have been prepared by entrapping TiO_2 within SiO_2 matrix through a simple sol−gel method under ambient temperature and pressure and first applied to photocatalytic CO_2 reduction with H_2O in gas-phase under simulated solar light irradiation. It has been found that TiO_2@SiO_2 composites exhibit higher photoactivity for CO_2 reduction compared with the non-entrapped TiO_2, which is attributed to the synergistic effects of the increased adsorption capacity toward CO_2 as well as the lengthened fate of electron−hole pairs in TiO_2@SiO_2 composites. In particular, the coating layer of silica over TiO_2 contributes to achieving high selectivity of CO formation during the photocatalytic reduction of CO_2, where the enriched density of adsorbed CO_2 on the reactive sites of the samples plays the crucial role. It is anticipated that our work could inspire ongoing interest in utilizing the SiO_2 coating method as well as other proper core−shell strategy to tune the activity and selectivity of semiconductor-based materials for artificial photoreduction of CO_2 to value-added solar fuels.

DOI: 10.1021/acs.jpcc.5b08893
J. Phys. Chem. C 2016, 120, 265−273

■ ASSOCIATED CONTENT

Supporting Information

The Supporting Information is available free of charge on the ACS Publications website at DOI: 10.1021/acs.jpcc.5b08893.

Photographs of the experimental setup for photocatalytic gas-phase CO_2 reduction and the quartz reactor, dimension distribution of the TiO_2 core and SiO_2 shell for TiO_2@30%SiO_2 composite, summary of the morphological characterization based on the N_2 adsorption−desorption isotherms and CO_2 adsorption isotherms, N_2 adsorption−desorption isotherms and PL lifetimes of all samples and O_2 evolved rate and stoichiometric rate of O_2 formation over TiO_2 and TiO_2@30%SiO_2 composites (PDF)

■ AUTHOR INFORMATION

Corresponding Author

*Phone +86 591 83779326. E-mail: yjxu@fzu.edu.cn.

Notes

The authors declare no competing financial interest.

■ ACKNOWLEDGMENTS

The support from the Key Project of National Natural Science Foundation of China (Grant U1463204), the National Natural Science Foundation of China (Grants 20903023 and 21173045), the Award Program for Minjiang Scholar Professorship, the Natural Science Foundation of Fujian Province for Distinguished Young Investigator Grant (No. 2012J06003), the Independent Research Project of State Key Laboratory of Photocatalysis on Energy and Environment (No. 2014A05), the first Program of Fujian Province for Top Creative Young Talents, and the Program for Returned High-Level Overseas Chinese Scholars of Fujian province is gratefully acknowledged.

■ REFERENCES

(1) Centi, G.; Perathoner, S. Opportunities and prospects in the chemical recycling of carbon dioxide to fuels. *Catal. Today* **2009**, *148*, 191−205.

(2) Dhakshinamoorthy, A.; Navalon, S.; Corma, A.; Garcia, H. Photocatalytic CO_2 reduction by TiO_2 and related titanium containing solids. *Energy Environ. Sci.* **2012**, *5*, 9217−9233.

(3) Hunt, A. J.; Sin, E. H.; Marriott, R.; Clark, J. H. Generation, capture, and utilization of industrial carbon dioxide. *ChemSusChem* **2010**, *3*, 306−322.

(4) Izumi, Y. Recent advances in the photocatalytic conversion of carbon dioxide to fuels with water and/or hydrogen using solar energy and beyond. *Coord. Chem. Rev.* **2013**, *257*, 171−186.

(5) Marszewski, M.; Cao, S.; Yu, J.; Jaroniec, M. Semiconductor-based photocatalytic CO_2 conversion. *Mater. Horiz.* **2015**, *2*, 261−278.

(6) Yuan, Y.-P.; Ruan, L.-W.; Barber, J.; Joachim Loo, S. C.; Xue, C. Hetero-nanostructured suspended photocatalysts for solar-to-fuel conversion. *Energy Environ. Sci.* **2014**, *7*, 3934−3951.

(7) Yu, J.; Low, J.; Xiao, W.; Zhou, P.; Jaroniec, M. Enhanced photocatalytic CO_2-reduction activity of anatase TiO_2 by coexposed {001} and {101} facets. *J. Am. Chem. Soc.* **2014**, *136*, 8839−8842.

(8) Li, Q.; Zong, L.; Li, C.; Yang, J. Photocatalytic reduction of CO_2 on MgO/TiO_2 nanotube films. *Appl. Surf. Sci.* **2014**, *314*, 458−463.

(9) Yu, J.; Wang, K.; Xiao, W.; Cheng, B. Photocatalytic reduction of CO_2 into hydrocarbon solar fuels over g-C_3N_4-Pt nanocomposite photocatalysts. *Phys. Chem. Chem. Phys.* **2014**, *16*, 11492−11501.

(10) Liu, S.; Yang, M.-Q.; Tang, Z.-R.; Xu, Y.-J. A nanotree-like CdS/ZnO nanocomposite with spatially branched hierarchical structure for photocatalytic fine-chemical synthesis. *Nanoscale* **2014**, *6*, 7193−7198.

(11) Yuan, L.; Xu, Y.-J. Photocatalytic conversion of CO_2 into value-added and renewable fuels. *Appl. Surf. Sci.* **2015**, *342*, 154−167.

(12) Rani, S.; Bao, N.; Roy, S. C. Solar spectrum photocatalytic Conversion of CO_2 and water vapor into hydrocarbons using TiO_2 nanoparticle membranes. *Appl. Surf. Sci.* **2014**, *289*, 203−208.

(13) Liu, L.; Li, Y. Understanding the reaction mechanism of photocatalytic reduction of CO_2 with H_2O on TiO_2-based photocatalysts: A review. *Aerosol Air Qual. Res.* **2014**, *14*, 453−469.

(14) Xie, S.; Wang, Y.; Zhang, Q.; Fan, W.; Deng, W.; Wang, Y. Photocatalytic reduction of CO_2 with H_2O: Significant enhancement of the activity of Pt-TiO_2 in CH_4 formation by addition of MgO. *Chem. Commun.* **2013**, *49*, 2451−2453.

(15) Liu, L.; Zhao, C.; Zhao, H.; Pitts, D.; Li, Y. Porous microspheres of MgO-patched TiO_2 for CO_2 photoreduction with H_2O vapor: Temperature-dependent activity and stability. *Chem. Commun.* **2013**, *49*, 3664−3666.

(16) Arai, T.; Sato, S.; Kajino, T.; Morikawa, T. Solar CO_2 reduction using H_2O by a semiconductor/metal-complex hybrid photocatalyst: Enhanced efficiency and demonstration of a wireless system using $SrTiO_3$ photoanodes. *Energy Environ. Sci.* **2013**, *6*, 1274−1282.

(17) Zhao, C.; Liu, L.; Zhang, Q.; Wang, J.; Li, Y. Photocatalytic conversion of CO_2 and H_2O to fuels by nanostructured Ce-TiO_2/SBA-15 composites. *Catal. Sci. Technol.* **2012**, *2*, 2558−2568.

(18) Li, K.; An, X.; Park, K. H.; Khraisheh, M.; Tang, J. A critical review of CO_2 photoconversion: Catalysts and reactors. *Catal. Today* **2014**, *224*, 3−12.

(19) Meng, X.; Wang, T.; Liu, L.; Ouyang, S.; Li, P.; Hu, H.; Kako, T.; Iwai, H.; Tanaka, A.; Ye, J. Photothermal conversion of CO_2 into CH_4 with H_2 over Group VIII nanocatalysts: An alternative approach for solar fuel production. *Angew. Chem.* **2014**, *126*, 11662−11666.

(20) Indrakanti, V. P.; Kubicki, J. D.; Schobert, H. H. Photoinduced activation of CO_2 on Ti-based heterogeneous catalysts: Current state, chemical physics-based insights and outlook. *Energy Environ. Sci.* **2009**, *2*, 745−758.

(21) Habisreutinger, S. N.; Schmidt-Mende, L.; Stolarczyk, J. K. Photocatalytic reduction of CO_2 on TiO_2 and other semiconductors. *Angew. Chem., Int. Ed.* **2013**, *52*, 7372−7408.

(22) Li, M.; Li, P.; Chang, K.; Wang, T.; Liu, L.; Kang, Q.; Ouyang, S.; Ye, J. Highly efficient and stable photocatalytic reduction of CO_2 to CH_4 over Ru loaded $NaTaO_3$. *Chem. Commun.* **2015**, *51*, 7645−7648.

(23) AlOtaibi, B.; Fan, S.; Wang, D.; Ye, J.; Mi, Z. Wafer-level artificial photosynthesis for CO_2 reduction into CH_4 and CO using GaN nanowires. *ACS Catal.* **2015**, *5*, 5342−5348.

(24) Liu, Q.; Zhou, Y.; Kou, J.; Chen, X.; Tian, Z.; Gao, J.; Yan, S.; Zou, Z. High-yield synthesis of ultralong and ultrathin Zn_2GeO_4 nanoribbons toward improved photocatalytic reduction of CO_2 into renewable hydrocarbon fuel. *J. Am. Chem. Soc.* **2010**, *132*, 14385−14387.

(25) Li, P.; Zhou, Y.; Li, H.; Xu, Q.; Meng, X.; Wang, X.; Xiao, M.; Zou, Z. Correction: All-solid-state Z-scheme system arrays of $Fe_2V_4O_{13}$/RGO/CdS for visible light-driving photocatalytic CO_2 reduction into renewable hydrocarbon fuel. *Chem. Commun.* **2015**, *51*, 800−803.

(26) Zhai, Q.; Xie, S.; Fan, W.; Zhang, Q.; Wang, Y.; Deng, W.; Wang, Y. Photocatalytic conversion of carbon dioxide with water into methane: Platinum and copper (I) oxide co-catalysts with a core-shell structure. *Angew. Chem.* **2013**, *125*, 5888−5891.

(27) Rasko, J.; Solymosi, F. Infrared spectroscopic study of the photoinduced activation of CO_2 on TiO_2 and Rh/TiO_2 catalysts. *J. Phys. Chem.* **1994**, *98*, 7147−7152.

(28) Shiraishi, Y.; Saito, N.; Hirai, T. Adsorption-driven photocatalytic activity of mesoporous titanium dioxide. *J. Am. Chem. Soc.* **2005**, *127*, 12820−12822.

(29) Xi, G.; Ouyang, S.; Ye, J. General synthesis of hybrid TiO_2 mesoporous "french fries" toward improved photocatalytic conversion of CO_2 into hydrocarbon fuel: A case of TiO_2/ZnO. *Chem. - Eur. J.* **2011**, *17*, 9057−9061.

(30) Yan, S. C.; Ouyang, S. X.; Gao, J.; Yang, M.; Feng, J. Y.; Fan, X. X.; Wan, L. J.; Li, Z. S.; Ye, J. H.; Zhou, Y.; Zou, Z. G. A room-

DOI: 10.1021/acs.jpcc.5b08893
J. Phys. Chem. C 2016, 120, 265−273

temperature reactive-template route to mesoporous $ZnGa_2O_4$ with improved photocatalytic activity in reduction of CO_2. *Angew. Chem.* **2010**, *122*, 6544−6548.
(31) Meng, X.; Ouyang, S.; Kako, T.; Li, P.; Yu, Q.; Wang, T.; Ye, J. Photocatalytic CO_2 conversion over alkali modified TiO_2 without loading noble metal cocatalyst. *Chem. Commun.* **2014**, *50*, 11517−11519.
(32) Ciriminna, R.; Fidalgo, A.; Pandarus, V.; Béland, F.; Ilharco, L. M.; Pagliaro, M. The sol-gel route to advanced silica-based materials and recent applications. *Chem. Rev.* **2013**, *113*, 6592−6620.
(33) Ciriminna, R.; Sciortino, M.; Alonzo, G.; Schrijver, A. d.; Pagliaro, M. From molecules to systems: Sol-gel microencapsulation in silica-based materials. *Chem. Rev.* **2011**, *111*, 765−789.
(34) Pagliaro, M.; Ciriminna, R.; Palmisano, G. The chemical effects of molecular sol−gel entrapment. *Chem. Soc. Rev.* **2007**, *36*, 932−940.
(35) Shang, L.; Bian, T.; Zhang, B.; Zhang, D.; Wu, L. Z.; Tung, C. H.; Yin, Y.; Zhang, T. Graphene-supported ultrafine metal nanoparticles encapsulated by mesoporous Silica: Robust catalysts for oxidation and reduction reactions. *Angew. Chem.* **2014**, *126*, 254−258.
(36) Ge, J.; Zhang, Q.; Zhang, T.; Yin, Y. Core-satellite nanocomposite catalysts protected by a porous silica shell: Controllable reactivity, high stability, and magnetic recyclability. *Angew. Chem.* **2008**, *120*, 9056−9060.
(37) Zhang, Y.; Ciriminna, R.; Palmisano, G.; Xu, Y.-J.; Pagliaro, M. Sol-gel entrapped visible light photocatalysts for selective conversions. *RSC Adv.* **2014**, *4*, 18341−18346.
(38) Wang, S.; Wang, T.; Chen, W.; Hori, T. Phase-selectivity photocatalysis: A new approach in organic pollutants' photodecomposition by nanovoid core (TiO_2)/shell (SiO_2) nanoparticles. *Chem. Commun.* **2008**, 3756−3758.
(39) Hu, S.; Li, F.; Fan, Z. Preparation of SiO_2-coated TiO_2 composite materials with enhanced photocatalytic activity under UV light. *Bull. Korean Chem. Soc.* **2012**, *33*, 1895−1899.
(40) Qin, X.; Jing, L.; Tian, G.; Qu, Y.; Feng, Y. Enhanced photocatalytic activity for degrading Rhodamine B solution of commercial Degussa P25 TiO_2 and its mechanisms. *J. Hazard. Mater.* **2009**, *172*, 1168−1174.
(41) Lassaletta, G.; Fernandez, A.; Espinos, J.; Gonzalez-Elipe, A. Spectroscopic characterization of quantum-sized TiO_2 supported on silica: Influence of size and TiO_2-SiO_2 interface composition. *J. Phys. Chem.* **1995**, *99*, 1484−1490.
(42) Mejias, J.; Jiménez, V.; Lassaletta, G.; Fernández, A.; Espinós, J.; González-Elipe, A. Interpretation of the binding energy and auger parameter shifts found by XPS for TiO_2 supported on different surfaces. *J. Phys. Chem.* **1996**, *100*, 16255−16262.
(43) Erdem, B.; Hunsicker, R. A.; Simmons, G. W.; Sudol, E. D.; Dimonie, V. L.; El-Aasser, M. S. XPS and FTIR surface characterization of TiO_2 particles used in polymer encapsulation. *Langmuir* **2001**, *17*, 2664−2669.
(44) Zhou, Z.; Zhu, L.; Li, J.; Tang, H. Electrochemical preparation of TiO_2/SiO_2 composite film and its high activity toward the photoelectrocatalytic degradation of methyl orange. *J. Appl. Electrochem.* **2009**, *39*, 1745−1753.
(45) Manzanares, M.; Fàbrega, C.; Ossó, J. O.; Vega, L. F.; Andreu, T.; Morante, J. R. Engineering the TiO_2 outermost layers using magnesium for carbon dioxide photoreduction. *Appl. Catal., B* **2014**, *150*, 57−62.
(46) Li, G.; Liu, F.; Zhang, Z. Enhanced photocatalytic activity of silica-embedded TiO_2 hollow microspheres prepared by one-pot approach. *J. Alloys Compd.* **2010**, *493*, L1−L7.
(47) Jafry, H. R.; Liga, M. V.; Li, Q.; Barron, A. R. Simple route to enhanced photocatalytic activity of P25 titanium dioxide nanoparticles by silica addition. *Environ. Sci. Technol.* **2011**, *45*, 1563−1568.
(48) Xu, Y.-h.; Zeng, Z.-x. The preparation, characterization, and photocatalytic activities of Ce-TiO_2/SiO_2. *J. Mol. Catal. A: Chem.* **2008**, *279*, 77−81.
(49) Liu, Y.; Zhou, S.; Li, J.; Wang, Y.; Jiang, G.; Zhao, Z.; Liu, B.; Gong, X.; Duan, A.; Liu, J.; et al. Photocatalytic reduction of CO_2 with water vapor on surface La-modified TiO_2 nanoparticles with enhanced CH_4 selectivity. *Appl. Catal., B* **2015**, *168*, 125−131.
(50) Seok, S. I.; Kim, J. H. TiO_2 nanoparticles formed in silica sol-gel matrix. *Mater. Chem. Phys.* **2004**, *86*, 176−179.
(51) Gao, X.; Wachs, I. E. Titania-silica as catalysts: molecular structural characteristics and physico-chemical properties. *Catal. Today* **1999**, *51*, 233−254.
(52) Liu, Z.; Crumbaugh, G. M.; Davis, R. J. Effect of structure and composition on epoxidation of hexenecatalyzed by microporous and mesoporous Ti-Si mixed oxides. *J. Catal.* **1996**, *159*, 83−89.
(53) Cheng, P.; Zheng, M.; Jin, Y.; Huang, Q.; Gu, M. Preparation and characterization of silica-doped titania photocatalyst through sol−gel method. *Mater. Lett.* **2003**, *57*, 2989−2994.
(54) Sasirekha, N.; Basha, S. J. S.; Shanthi, K. Photocatalytic performance of Ru doped anatase mounted on silica for reduction of carbon dioxide. *Appl. Catal., B* **2006**, *62*, 169−180.
(55) Murashkevich, A.; Lavitskaya, A.; Barannikova, T.; Zharskii, I. Infrared absorption spectra and structure of TiO_2-SiO_2 composites. *J. Appl. Spectrosc.* **2008**, *75*, 730−734.
(56) Sasahara, A.; Pang, C. L.; Tomitori, M. Atomic scale analysis of ultrathin SiO_2 films prepared on TiO_2 (100) surfaces. *J. Phys. Chem. C* **2010**, *114*, 20189−20194.
(57) Xi, G.; Ouyang, S.; Li, P.; Ye, J.; Ma, Q.; Su, N.; Bai, H.; Wang, C. Ultrathin $W_{18}O_{49}$ Nanowires with diameters below 1 nm: Synthesis, near-infrared absorption, photoluminescence, and photochemical reduction of carbon dioxide. *Angew. Chem., Int. Ed.* **2012**, *51*, 2395−2399.
(58) Hurum, D. C.; Agrios, A. G.; Gray, K. A.; Rajh, T.; Thurnauer, M. C. Explaining the enhanced photocatalytic activity of Degussa P25 mixed-phase TiO_2 using EPR. *J. Phys. Chem. B* **2003**, *107*, 4545−4549.
(59) Hurum, D. C.; Gray, K. A.; Rajh, T.; Thurnauer, M. C. Recombination pathways in the Degussa P25 formulation of TiO_2: Surface versus lattice mechanisms. *J. Phys. Chem. B* **2005**, *109*, 977−980.
(60) Ide, Y.; Koike, Y.; Ogawa, M. Molecular selective photocatalysis by TiO_2/nanoporous silica core/shell particulates. *J. Colloid Interface Sci.* **2011**, *358*, 245−251.
(61) Yu, G.; Geng, L.; Wu, S.; Yan, W.; Liu, G. Highly-efficient cocatalyst-free H_2-evolution over silica-supported CdS nanoparticle photocatalysts under visible light. *Chem. Commun.* **2015**, *51*, 10676−10679.
(62) Arun Kumar, D. A.; Xavier, J. A.; Shyla, J. M.; Xavier, F. P. Synthesis and structural, optical and electrical properties of TiO_2/SiO_2 nanocomposites. *J. Mater. Sci.* **2013**, *48*, 3700−3707.
(63) Sing, K.; Everett, D.; Haul, R.; Moscou, L.; Pierotti, R.; Rouquerol, J.; Siemieniewska, T. Reporting physisorption data for gas/solid systems with special reference to the determination of surface area and porosity (Recommendations 1984). *Pure Appl. Chem.* **1985**, *57*, 603−619.
(64) Li, Y.; Wang, W.-N.; Zhan, Z.; Woo, M.-H.; Wu, C.-Y.; Biswas, P. Photocatalytic reduction of CO_2 with H_2O on mesoporous silica supported Cu/TiO_2 catalysts. *Appl. Catal., B* **2010**, *100*, 386−392.
(65) Hou, Y.; Li, X.; Zhao, Q.; Quan, X.; Chen, G. TiO_2 nanotube/Ag-AgBr three-component nanojunction for efficient photoconversion. *J. Mater. Chem.* **2011**, *21*, 18067−18076.
(66) Wang, W.-N.; Park, J.; Biswas, P. Rapid synthesis of nanostructured Cu-TiO_2-SiO_2 composites for CO_2 photoreduction by evaporation driven self-assembly. *Catal. Sci. Technol.* **2011**, *1*, 593−600.
(67) Yuan, L.; Yang, M.-Q.; Xu, Y.-J. A low-temperature and one-step method for fabricating $ZnIn_2S_4$-GR nanocomposites with enhanced visible light photoactivity. *J. Mater. Chem. A* **2014**, *2*, 14401−14412.
(68) Han, C.; Yang, M.-Q.; Zhang, N.; Xu, Y.-J. Enhancing the visible light photocatalytic performance of ternary CdS-(graphene-Pd) nanocomposites via a facile interfacial mediator and co-catalyst strategy. *J. Mater. Chem. A* **2014**, *2*, 19156−19166.

DOI: 10.1021/acs.jpcc.5b08893
J. Phys. Chem. C 2016, 120, 265−273